Computational Materials Science 160 (2019) 207–216

Contents lists available at ScienceDirect

Computational Materials Science

journal homepage: www.elsevier.com/locate/commatsci

Rising Stars in Computational Materials Science

Pushing the frontiers of modeling excited electronic states and dynamics to accelerate materials engineering and design

Kisung Kang[a], Alina Kononov[b], Cheng-Wei Lee[a], Joshua A. Leveillee[a], Ethan P. Shapera[b], Xiao Zhang[c], André Schleife[a,d,e,*]

[a] Department of Materials Science and Engineering, University of Illinois at Urbana-Champaign, Urbana, IL 61801, USA
[b] Department of Physics, University of Illinois at Urbana-Champaign, Urbana, IL 61801, USA
[c] Department of Mechanical Science and Engineering, University of Illinois at Urbana-Champaign, Urbana, IL 61801, USA
[d] Frederick Seitz Materials Research Laboratory, University of Illinois at Urbana-Champaign, Urbana, IL 61801, USA
[e] National Center for Supercomputing Applications, University of Illinois at Urbana-Champaign, Urbana, IL 61801, USA

ARTICLE INFO

Keywords:
Many-body perturbation theory
Time-dependent density functional theory
Database
Semiconductors
Metals

ABSTRACT

Electronic excitations and their dynamics are oftentimes at the foundation of how we use and probe materials. While recent experimental advances allow us to do so with unprecedented accuracy and time resolution, their interpretation relies on solid theoretical understanding. This can be provided by cutting-edge, first-principles theoretical-spectroscopy based on many-body perturbation theory (MBPT) and time-dependent density functional theory (TDDFT). In this work we review some of our recent results as successful examples for how electronic-structure methods lead to interesting insight into electronic excitations and deep understanding of modern materials. In many cases these techniques are accurate and even predictive, yet they rely on approximations to be computationally feasible. We illustrate the need for further theoretical understanding, using dielectric screening as an example in MBPT and faster, more accurate numerical integrators as a challenge for real-time TDDFT. Finally, we describe how incorporating online databases into computational materials research on excited electronic states can side-step the problem of high computational cost to facilitate materials design.

1. Introduction

Materials are real-world realizations of quantum mechanics, embodying what is described as interactions in a Hamiltonian. Novel states of matter emerge, depending on relative coupling strengths of these interactions as well as external excitations. An intricate interplay of charge, spin, orbital, and lattice degrees of freedom and excitations determines underlying time scales and, hence, real-time dynamics. In particular, excitations of electrons out of their ground state are at the heart of how we interact with materials; they are used to probe properties and underlie applications (see Fig. 1). Intriguing and rich information about electrons and ions of a material is encoded in these excitations that are dominated by quantum-mechanical effects. For instance, the emergence of exotic quantum states, such as the recently discovered condensation of excitons in a transition-metal dichalcogenide [1], challenge the limits of our fundamental understanding of nature at microscopic length and ultrafast time scales.

Fortunately, we are currently on the verge of pushing experiment and simulation into a spatial and temporal regime that allows studying and manipulating excited quantum states. Increasingly sophisticated experimental techniques enable control of electronic motion on atto-second time scales and study of implications for concomitant ion dynamics [2]. At the same time, interpretation of such experiments relies on theoretical insight, rendering this an ideal time for making progress with first-principles computational approaches. In addition to advancing fundamental knowledge, the discovery, manipulation, and design of electronic excitations can provide technological breakthroughs for critical applications of societal importance. Prominent examples include e.g. quantum information processing, next-generation energy-conversion, energy-storage, and catalytic systems.

Obtaining a thorough understanding of, and achieving control over, individual couplings and their time scales, however, remains in its infancy. From a theoretical point of view, this largely can be attributed to the highly non-trivial and fundamentally challenging mathematical description of many-body interactions via the Schrödinger equation, a multi-dimensional partial differential equation [3]. Consequently, a quantitatively accurate theoretical description requires reliable physical and numerical approximations to the quantum-mechanical many-electron problem, as well as coupling to ions and spins.

* Corresponding author.
E-mail address: schleife@illinois.edu (A. Schleife).

https://doi.org/10.1016/j.commatsci.2019.01.004
Received 1 November 2018; Received in revised form 31 December 2018; Accepted 4 January 2019

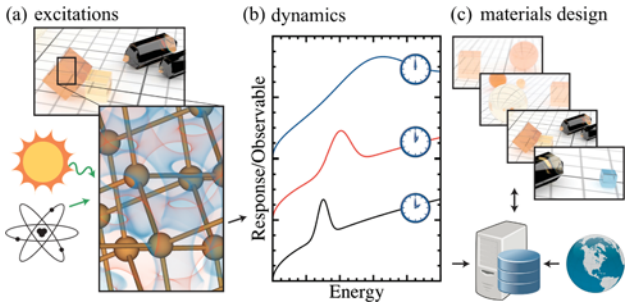

Fig. 1. (a) Electronic excitations are created in materials, e.g. by optical or particle radiation. (b) Material properties can be probed with high time resolution through excited electronic states and their dynamics. (c) This information, along with other material properties collected in online databases, can be used to facilitate materials design.

At the same time, progress in understanding modern problems of condensed-matter physics is promising, as it is deeply connected to grand challenges at the forefront of contemporary materials science: The above example of exciton condensation [1] impressively illustrates how intricate effects in quantum materials are intimately tied to excited electronic states in a semiconductor. However, studying novel and modern materials, oftentimes with large numbers of atoms and electrons in a unit cell, renders quantum-mechanical calculations challenging. In practice, density functional theory [4–7] (DFT) and its time-dependent (TD) complement, TDDFT [8], play a central role for obtaining electronic structure and real-time dynamics. Many-body perturbation theory (MBPT) improves the description of the electron-electron interaction over DFT and takes electronic excitations into account in a systematic way [9]. These techniques and their practical implementations are increasingly advanced, oftentimes exploiting modern high-performance supercomputers, enabling deep understanding that complements experiments. However, the utility of quantum-mechanical first-principles calculations critically depends on how underlying approximations balance accuracy and computational cost.

In this review paper, we discuss recent and ongoing efforts in applying first-principles techniques to study excited electronic states and their real-time dynamics. We illustrate our successes in using MBPT to establish structure-property relationships and present insight from TDDFT into ultrafast electron-ion dynamics. In some cases, our work exposed the need for improving the underlying approximations. We outline our path towards such improvements and discuss our ongoing work in this direction. Finally, we explain our vision of incorporating information from online databases to address the high computational cost of cutting-edge first-principles techniques in the context of materials design (see Fig. 1). It is the right time for this exciting endeavor, as the advent of high-performance supercomputers and materials databases allows for sophisticated, accurate computational work that will break ground for novel applications in materials science for the benefit of society.

2. Many-body perturbation theory: electronic structure and optical properties

Electronic structure is probed experimentally using excitation mechanisms with energies large enough to remove electrons from materials. Analyzing the energy or momentum distribution of these electrons provides valuable insight into materials via band structure and density of states. From first principles, MBPT is a successful and widely used framework to describe these electronic single-particle excitations and explicitly accounts for the response of the material's electronic system to the removal of an electron upon excitation [9]. Using the quasiparticle (QP) picture, MBPT can accurately predict excitation energies in excellent agreement with experiment. In particular, within MBPT electronic QP excitations can be described using a Dyson equation,

$$\left[-\frac{\hbar^2\nabla^2}{2m}+\hat{V}_{\text{ext}}\left(\mathbf{r},\mathbf{R}\right)+V_{\text{H}}(\mathbf{r})\right]\psi^{\text{QP}}_{n\mathbf{k}}(\mathbf{r})+\int d\mathbf{r}'\Sigma\left(\mathbf{r}\mathbf{r}',\varepsilon^{\text{QP}}_{n\mathbf{k}}/\hbar\right)\psi^{\text{QP}}_{n\mathbf{k}}(\mathbf{r}') = \varepsilon^{\text{QP}}_{n\mathbf{k}}\psi^{\text{QP}}_{n\mathbf{k}}(\mathbf{r}), \quad (1)$$

where $\varepsilon^{\text{QP}}_{n\mathbf{k}}$ and $\psi^{\text{QP}}_{n\mathbf{k}}(\mathbf{r})$ are QP energies and wave functions, respectively, of single-particle states labeled by band (n) and $\mathbf{k}$-point index. $\hat{V}_{\text{ext}}(\mathbf{r},\mathbf{R})$ is the external potential due to ions, $V_{\text{H}}(\mathbf{r})$ describes the Hartree electron-electron interaction, and $\mathbf{r}$ and $\mathbf{R}$ are electronic and ionic spatial coordinates, respectively.

The central term in Eq. (1) is the electronic self energy Σ that describes electron-electron interactions beyond Hartree and needs to be approximated in practice. Hedin's *GW* approximation is extremely common and very successful (see Refs. [10,11] and references therein for a more comprehensive introduction). It expresses Σ as a product of the Green's function G of the electronic system and the screened Coulomb electron-electron interaction W. In practice, a fully self-consistent solution of Eq. (1) is computationally infeasible, and instead perturbation theory is used. This provides QP corrections of starting-point single-particle excitation energies obtained from a more affordable approach with a simpler description of the electron-electron interaction. DFT with a local [6], semi-local [7], or hybrid-functional [12,13] approximation for exchange and correlation can provide such a starting point. While QP energies oftentimes explain electronic structure of materials in very good agreement with experiment, they are also an important ingredient to investigate optical properties.

Optical excitations due to photons in or near the visible spectral range carry too little energy to *remove* electrons from materials that absorb the photon. Instead, electrons participating in optical absorption are excited into the conduction band, leaving behind holes in the valence band, which corresponds to a two-particle excitation. Electrons and holes bind to each other due to their opposite charges and form electron-hole pairs, i.e. excitons. Properties of excitons can dominate absorption spectra and, hence, applications of materials: Take photovoltaics, for instance, where strongly bound excitons are less desirable than weakly bound ones that are easily separated by built-in fields in semiconductor devices.

A possible route to study two-particle excitations is again to use MBPT, in which case a Bethe-Salpeter equation (BSE) for the optical polarization function needs to be solved [9]. In practice, the BSE is rewritten as an eigenvalue problem with an excitonic Hamiltonian,

$$H(cv\mathbf{k},c'v'\mathbf{k}') = (\varepsilon^{\text{QP}}_{c\mathbf{k}}-\varepsilon^{\text{QP}}_{v\mathbf{k}})\delta_{cc'}\delta_{vv'}\delta_{\mathbf{k}\mathbf{k}'}-\Xi(cv\mathbf{k},c'v'\mathbf{k}'), \quad (2)$$

where $\Xi(cv\mathbf{k},c'v'\mathbf{k}')$ contains the screened Coulomb electron-hole interaction W and unscreened electron-hole exchange terms [9]. $cv\mathbf{k}$ are valence (v), conduction (c), and $\mathbf{k}$-point index of a non-interacting electron-hole pair. After computing this Hamiltonian we either use a time-propagation technique [14,15] to obtain the complex, frequency-dependent dielectric function, or a conjugate-gradient approach [16] to compute lowest eigenvalues and, thus, exciton-binding energies.

DFT and *GW* calculations discussed here were carried out using the Vienna *Ab-initio* Simulation Package [17–20] (VASP). BSE calculations of optical properties are computationally challenging due to the requirement for dense $\mathbf{k}$-point grids and large numbers of empty states. We used the implementation described in Refs. [16,21], which reads Kohn-Sham (KS) wave functions and optical matrix elements from VASP. It is extremely well-suited for converged studies of optical properties: By using a model dielectric function [22] it evaluates W in the excitonic Hamiltonian very quickly, allowing us to use very dense as well as hybrid $\mathbf{k}$-point meshes [16].

Over the last years we used this predictive computational approach to understand the quantum-mechanical electron-electron interaction and excited-state properties, in particular for oxide [23–29] and nitride [30,31] semiconductors. We studied QP band structures and densities

of states, the influence of spin-orbit coupling, as well as optical-absorption and electron-loss spectra, including exciton binding energies. In particular, we precisely explained valence-band splittings in equilibrium and non-equilibrium crystal structures as observed by thorough optical spectroscopy experiments on oxides [32] and nitrides [33]. We also combined MBPT with a cluster expansion technique for alloys [34–39]. From this we predicted how different cation distributions, arising from different thermodynamic conditions during sample growth, may be exploited to engineer specific electronic and optical properties. For TiO_2 [34] we found that strong optical absorption can be induced in the sub-gap energy range by means of symmetry breaking via sulfur impurities. Finally, we showed that oxygen vacancies in MgO [40] lead to a strong peak in the absorption spectrum, the width of which is fundamentally determined by electron-phonon coupling.

More recently, our calculations [41] for two transparent conducting oxides, In_2O_3 and Ga_2O_3, revealed significant excitonic red shift and spectral redistribution due to electron-hole binding, as well as strong optical anisotropy in Ga_2O_3. Furthermore, for lanthanum aluminum oxide we showed that the position of the unoccupied La4*f* orbital within the conduction band critically determines the dielectric function of the material and QP effects are crucial to explain experimental data [42]. Our work on $K_2Sn_3O_7$ explained its behavior as a wide band gap semiconductor. This material shows a unique orthorhombic structure type among oxides and we predicted band structure, density of states, and optical properties [43]. Finally, we also recently employed MBPT to understand excitonic effects in scintillator materials [44–46], in which excitons can be produced as a result of high-energy radiation. We studied dielectric and electron-energy loss functions, which help to understand whether excitonic effects dominate the spectral properties of the emitted light and, thus, the energy resolution of the scintillator.

This variety of semiconductors illustrates diverse and interesting examples where we used MBPT to obtain detailed understanding of electronic structure and optical properties. More importantly, this constitutes an important foundation from which two promising research directions have emerged, that will be discussed next: First, in Section 3, we illustrate our current efforts to apply highly accurate first-principles calculations towards better understanding of structure-property relationships. In particular, we elucidate the relation of atomic geometries, chemical trends, and magnetic ordering with electronic and optical properties. Second, since an accurate description of dielectric screening is crucial for the success of MBPT, we outline our ongoing theoretical developments in Section 4.

3. Atomic geometries, chemical trends, and magnetic ordering

As an excellent example of the success of modern first-principles simulations, we used our expertise with characterizing optical properties to tie these to material composition and atomic geometry. We show that theoretical spectroscopy is now accurate enough to allow direct conclusions about structural properties and even phase identification. In particular, we discuss unique optical signatures for two examples: Using first-principles simulations for ZnO, we identify wurtzite (WZ) vs. boron-nitride (BN) polymorphs, and for CdSe we reliably distinguish between WZ and zinc-blende structures. This addresses the challenge of using simple and accurate optical analysis for crystal-type distinction. In addition, this approach is compatible with high-throughput experimentation as well as liquid-dispersed nano-materials. We envision that this capability will lead to design of better materials for applications including optoelectronics, shape- and size-tunable optical spectra of semiconductor nanocrystals for bioimaging, and strongly absorbing organo-metal halide perovskites for photovoltaics.

The first example focuses on a comparison of equilibrium WZ-ZnO and the non-equilibrium non-polar BN phase of ZnO (see Fig. 2) that has been reported for thin films and nanostructures. The BN phase is particularly interesting, as it provides a possible route to avoid dipoles that occur at (0001) surfaces of WZ-ZnO [48–50]. Until recently, its properties were not well-understood, largely because experimental and first-principles results for the atomic geometry could not be reconciled [51–54]. We explained electronic and optical properties of both phases, taking single-QP and excitonic effects into account by means of hybrid functionals as well as the *GW*-BSE approach [47], leading to a consistent picture based on first-principles theoretical spectroscopy. We specifically show that the band-gap difference of about 0.2 eV between BN-ZnO and WZ-ZnO agrees very well with experiment, assuming lattice coordinates from first-principles theory [51–55]. We also show that this result does not strongly depend on the approximation used for exchange and correlation, which we interpret as indication that the theoretical lattice geometry is indeed accurate.

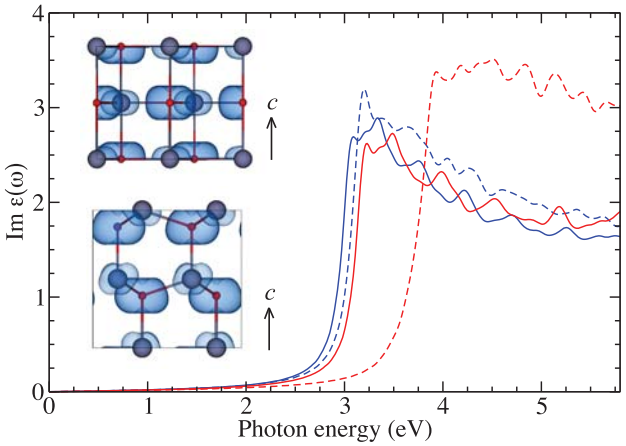

Fig. 2. Imaginary part of the dielectric function of WZ-ZnO (blue curves) and BN-ZnO (red curves) for ordinary ($\mathbf{E} \perp c$, solid curves) and extraordinary ($\mathbf{E} \parallel c$, dashed curves) light polarization. The insets show the partial charge density of the valence band maximum at the Γ point for BN-ZnO (top) and wurtzite-ZnO (bottom). The isosurface is chosen such that 90% of the electrons lie within [47].

In order to provide guidance for identifying both phases, we focus on optical anisotropy: BN-ZnO is optically more anisotropic than WZ-ZnO (see Fig. 2) and polarized light can be used to detect this difference. Furthermore, measurements using unpolarized light would lead to a two-step onset of optical absorption in BN-ZnO, with a clear energy separation of 0.5 eV. This separation is an order of magnitude smaller in WZ-ZnO (see Fig. 2), illustrating how optical-absorption spectra can be used to distinguish both polymorphs. In addition, we used the transfer-matrix method [56,57] to solve Maxwell's equations for thin films that are composed of both polymorphs. From these results we conclude the possibility of *tuning* optical properties, e.g. for nanostructures and thin films in UV detectors and UV protection, by incorporating purposefully designed fractions of BN-ZnO and WZ-ZnO into samples.

A similar approach enabled us to unravel optical properties of semiconductor nanocrystals [58]. These are extremely interesting for optoelectronics as well as bioimaging owing to their characteristic and highly tunable optical properties. While these properties are closely tied to the underlying crystal structure, standard crystallographic characterization is difficult, in particular when nanocrystals are small or polytypic, as diffraction can yield ambiguous phase signatures. Furthermore, these diffraction-based techniques are usually low-throughput and incompatible with samples in solution.

In a close collaboration with experiment, we recently combined absorption spectroscopy with first-principles electronic-structure theory: We reported unambiguous optical signatures that can be traced back to cubic (zinc-blende) and hexagonal (WZ) CdSe phases [58]. They appear in the ultraviolet photon energy range, i.e. above the absorption onset, and allow for rapid identification of phase, leading to simple and accurate crystallographic analysis for liquid-dispersed nanomaterials. We envision that this may help to better understand and engineer polytypic nanocrystals with different phase contributions and

underlying reactions during synthesis and processing, including high-throughput experimentation. We are currently working on extending this approach to extract information beyond size and phase from spectra, including shape, surface facets, and defects. We envision that this will pave the way towards the exciting prospect of designing precise optical features, optimized for specific applications via engineering of nanocrystal structure.

Recently, we also established a connection between optical properties and *chemical* trends: For two layered hybrid halide perovskites with different representative single-ring conjugated organic spacers we explored how different halogens, $X = \{\mathrm{I}, \mathrm{Br}, \mathrm{Cl}\}$, affect optical absorption [59]. These materials are interesting for device applications as they allow for low-cost engineering of chemical properties in order to design excitonic effects, optical absorption and emission, as well as charge-carrier transport properties [60–62]. We specifically used MBPT to explore excited-electron properties in ammonium-propyl-imidazole(API)-PbX_4 (see Fig. 3) and 2-phenethylammonium (PEA)-PbX_4 [59]. Fig. 3 illustrates the chemical trend of increasing band gaps and decreasing absorption at higher photon energies along the $X = \{\mathrm{I}, \mathrm{Br}, \mathrm{Cl}\}$ series.

For these materials we also showed that π and π^* states appear only further away from band extrema. This implies that absorption of visible light occurs primarily within the PbX_4 octahedral layers and electron-hole separation *between* layers requires UV light absorption. This implies that the π–π^* gap of the conjugated groups needs to be reduced, e.g. by adding more of the conjugated groups to the system. In addition, orbital overlap between layers must be increased to achieve larger transition dipole matrix elements for inter-layer absorption. This may be possible via including heavier elements in the organic layer. Furthermore, higher absorption of visible light and better mobilities are targets for materials design of these systems. In our ongoing work, we use accurate first-principles simulations to achieve these goals and to enable photo-induced charge separation and optoelectronic applications.

Finally, we also used modern first-principles simulations to explore the interaction of light and spin in antiferromagnetic materials: The topological metal-insulator transition (MIT) of antiferromagnetic materials and their semi-metallic behavior are attracting attention because of their implications for the electronic structure [63] and possible applications in future memory technologies. Hence, electrical switching mechanisms for antiferromagnets are proposed and attempts are made to understand the MIT [64]. In our work, we used DFT to study how the orientation of the Néel vector affects the magnetic symmetry of CuMnAs, possibly leading to the opening of a gap in the QP spectrum [65]. To this end, Fig. 4 shows part of our band structure data, which we used to verify model-Hamiltonian results.

We confirm for CuMnAs that a gap in the band structure can open, depending on the antiferromagnetic ordering and the associated non-symmorphic symmetry [65]. Since the different orderings and, thus, gapped and gapless phase, have different free energies, these results can be

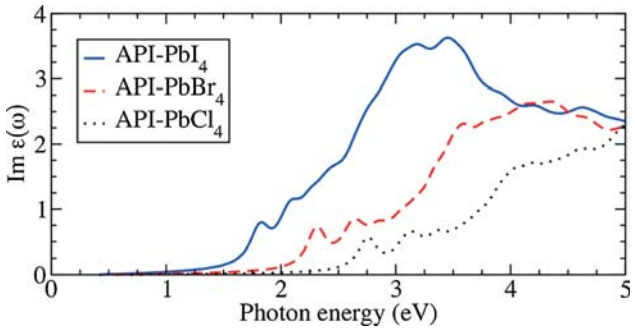

Fig. 3. Imaginary part of the dielectric function of API-PbI_4, API-PbBr_4, and API-PbCl_4, including excitonic effects. The absorption onset is attributed to optical transitions within the perovskite layer; the organic layer contributes only in the UV range.

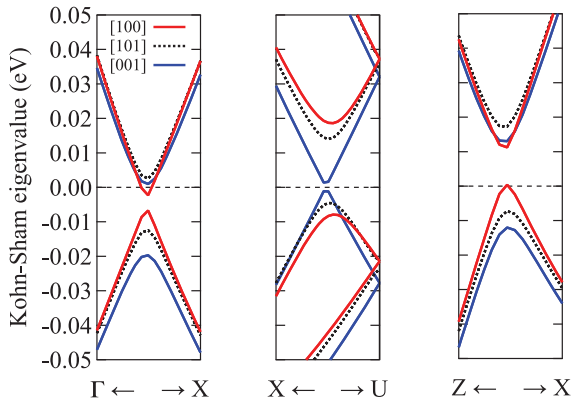

Fig. 4. KS band structure of CuMnAs from DFT-PBE calculations, for three different Néel vector orientations. It can be seen that there is a Dirac point between X and U in the Brillouin zone if the Néel vector is oriented parallel to the [001] direction.

connected to the position of the electron chemical potential, indicating that a (semi)metal-insulator transition may be induced by controlling the chemical potential in the material. While the gapped spectrum occurs when the chemical potential is at the Dirac point, the difference of the free energies reduces as the chemical potential deviates from this point. Hence, antiferromagnetic order can be switched from out-of-plane to in-plane by manipulating the chemical potential. This may open up applications related to voltage-induced switching of the Néel vector [65].

4. Developments around dielectric screening

In order for first-principles simulations to be accurate enough to reliably inform structure-property relationships, they must be based on accurate approximations. This requires precise lattice geometries and, as shown in Section 3, inclusion of QP and excitonic effects. While we illustrated above that MBPT successfully achieves this, we emphasize that *dielectric screening* of the electron-electron interaction is a critical and important quantity in this framework. Fundamentally, this can be expected, since the central *GW* approximation corresponds to a first-order expansion of the electronic self energy Σ in terms of the Green's function G and *screened* Coulomb interaction W [11]. We now discuss examples that, over the last years, have led us to realize this in the context of optical properties and outline our efforts to improve the theoretical description of dielectric screening.

In an ideal bulk material with nuclei assumed fixed within the Born-Oppenheimer approximation [66], only the electronic system gives rise to a polarizability, which contributes to dielectric screening. Hence, only electronic dielectric screening is typically evaluated to obtain the screened Coulomb interaction W. For this, the random-phase approximation [67] and DFT are commonly used; model dielectric functions are faster, approximate alternatives. Over the past years, we repeatedly showed how sensitively electronic screening affects electronic and optical properties: For ZnO we discussed that strain directly modifies dielectric screening, which impacts QP energies, band gap, and exciton binding energies [68]. Similarly, for a carbon nanotube we showed that a strain contribution to dielectric screening is significant, in addition to the usual strain-related deformation-potential picture [69].

This illustrates that an accurate description of electronic screening is crucial; however, in addition, other screening mechanisms can contribute in real materials: One example is doped systems [70–72], in which free carriers modify the dielectric tensor (see Fig. 5). In Ref. [73] we approximated this additional intraband screening due to free electrons via a static, wave-vector dependent Lindhard dielectric

$$\varepsilon_{\mathrm{intra}}(q) = 1 + \frac{e^2}{\varepsilon_0\,\varepsilon_{\mathrm{eff}}\,q^2}\frac{2n_c}{3\varepsilon_{\mathrm{F}}}\left[\frac{1}{2} + \frac{4k_{\mathrm{F}}^2 - q^2}{8k_{\mathrm{F}}\,q}\ln\left|\frac{2k_{\mathrm{F}} + q}{2k_{\mathrm{F}} - q}\right|\right]. \tag{3}$$

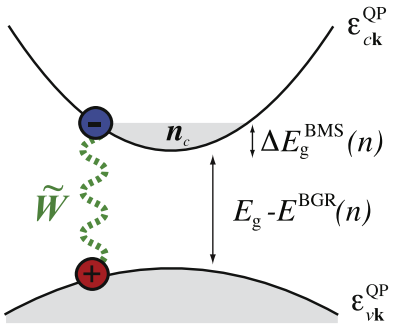

Fig. 5. Illustration of an electron-hole pair in a two-band model ($\varepsilon_{c\mathbf{k}}^{\mathrm{QP}}$, $\varepsilon_{v\mathbf{k}}^{\mathrm{QP}}$), bound by screened Coulomb interaction $\widetilde{W}$, in the presence of free electrons of concentration n_c. Band-gap renormalization due to the free electrons reduces the gap. Burstein-Moss shift causes the optical-absorption onset to shift to higher energies.

The free-electron concentration in the lowest conduction band is n_c and related to the Fermi wave vector $k_{\mathrm{F}} = \sqrt[3]{3\pi^2 n_c}$ and the Fermi energy $\varepsilon_{\mathrm{F}} = \hbar^2 k_{\mathrm{F}}^2/(2m_c)$ relative to the conduction-band minimum. Since small wave vectors dominate Eq. (3), we used the following small-q limit for wave-vector dependent screening [73,74]

$$\varepsilon(q) = \varepsilon_{\mathrm{eff}}\,\varepsilon_{\mathrm{intra}}(q) \approx \varepsilon_{\mathrm{eff}}\left(1 + \frac{q_{\mathrm{TF}}^2}{q^2}\right), \tag{4}$$

with the Thomas-Fermi (TF) wave vector

$$q_{\mathrm{TF}} = \sqrt{\frac{3n_c e^2}{2\,\epsilon_0\,\varepsilon_{\mathrm{eff}}\,\varepsilon_{\mathrm{F}}}}. \tag{5}$$

We then showed that taking into account this additional screening, as well as Pauli blocking and band-gap renormalization due to free carriers (see Fig. 5), leads to a highly accurate description of optical absorption and exciton binding in doped ZnO [75].

Another example for dielectric screening beyond purely electronic terms is that of *polar* materials. In these, the lattice shows a large polarizability, leading to an additional contribution to the dielectric tensor [76–79]. Its dependence on frequency and wave-vector needs to be analyzed to understand whether it is important for optical excitations. In the case of the BSE, where screening is typically restricted to a static, frequency-independent approximation, the importance of frequency dependence can be assessed via a comparison of exciton binding energies and longitudinal-optical (LO) phonon frequencies [80,81]. Static screening is sufficient when exciton binding energies are far from LO phonon frequencies, but the validity of the static approximation becomes questionable when they are comparable [81]. The same authors reported that electronic dominates over lattice screening when both dielectric constants are comparable [80], however, the wave-vector dependence also needs to be investigated in detail to develop a better understanding.

To shed further light onto this question, we study such polar materials that are defined by a large splitting of longitudinal- and transverse-optical phonon frequencies and, hence, a large difference between static and static electronic dielectric constants [77,82]. Many transparent conducting oxides are examples where this is the case (see Table 1 in Ref. [83]), but also perovskite materials, including organo-metal halides [84–86]. In Ref. [83] we showed that exciton-binding energies are close to LO phonon frequencies for polar materials and we compared highly accurate theoretical spectroscopy results to experimental data for cubic bixbyite In_2O_3. We illustrated the interplay of QP and excitonic effects across a large photon-energy range and reported excellent agreement between theory and experiment. We specifically showed that a lattice contribution to dielectric screening may determine the exciton binding energy and line shape near the absorption onset.

These cases exemplify how crucial an accurate description of dielectric screening is for the success of MBPT. We are currently working on providing better theoretical understanding to capture lattice polarizability and the associated screening dynamics, e.g. in systems where the approximation of fixed nuclei breaks down. We also work on improving the numerical implementation, both to mitigate high computational cost associated with studies of modern materials, such as complex polar oxides and perovskites, and to optimally exploit modern, massively parallel and hybrid computing paradigms, including traditional central-processing units, graphic chips, and many integrated cores. Within a collaboration, we accelerate the iterative diagonalization of the excitonic Hamiltonian, Eq. (2), by using the ChASE library [87]. We also note other efforts in this context [88] and envision that such developments improve the accuracy of MBPT and broaden its applicability both towards more diverse material systems and towards being used more routinely within the computational materials community.

5. Ultrafast electron-ion dynamics and electronic stopping

The previous section briefly alluded to the fixed-ion approximation becoming problematic and we now take this thought a step further: Scenarios in which the electronic system cannot be assumed in its ground state on the time scale of ionic motion are becoming increasingly accessible to experiment and, thus, of practical importance. Hence, for many novel phenomena across a wide range of technological applications—ranging from photocatalytic cells to radiation shielding in space—neglecting quantum dynamics of electrons renders important material properties inaccessible. Consequently, an accurate description of electron dynamics through TD quantum-mechanical theory is one of the most pressing challenges in computational materials science today.

Thanks to the Runge-Gross theorem [8], TDDFT has emerged as an accurate yet affordable route to investigate quantum dynamics of electrons in complex systems [89,90]. Going beyond the widely-used linear-response frequency-domain formulation, real-time TDDFT (RT-TDDFT) is becoming increasingly popular for studying excited-electron dynamics and has been applied to phenomena in chemistry, physics, and materials science. In the following, we review our recent work on ion irradiation as an important application of RT-TDDFT.

Our interest in energetic particle radiation is motivated by precisely engineered quantum bits via ion implantation, defect dynamics under radiation conditions, and electron equilibration in two-dimensional materials. In this context, our work, along with that of other groups [91–98], has paved the way towards a quantitative understanding of electronic stopping: Specific examples include stopping of light projectiles in metals such as aluminum [99], copper [100], and gold [101], as well as non-metals such as silicon [92], LiF [102], HfO_2 [103], and InP/GaP [104]. In particular, we showed that RT-TDDFT accurately describes electronic stopping of light projectile atoms in metallic [99,101] and semiconducting [104] targets over a wide range of projectile velocities. Without making assumptions about the dielectric functions of target materials or introducing ad hoc parameters such as effective charges, we showed that this approach accurately simulates electronic stopping, allowing for quantitative comparison with experiment.

Initially, we explored stopping in metals: For proton and helium projectiles in aluminum, our simulations provided a means of disentangling electronic-stopping contributions due to tightly bound semi-core electrons from geometric aspects of the projectile trajectory, such as channeling versus off-channeling, over a wide range of projectile velocities [99]. We also derived a scheme to study off-channeling projectiles using a long enough time average for a projectile that moves along a random direction through the target material with fixed velocity [99]. We then extended this work towards stopping of proton projectiles in gold [101] and again found excellent quantitative agreement with results from “The Stopping and Range of Ions in

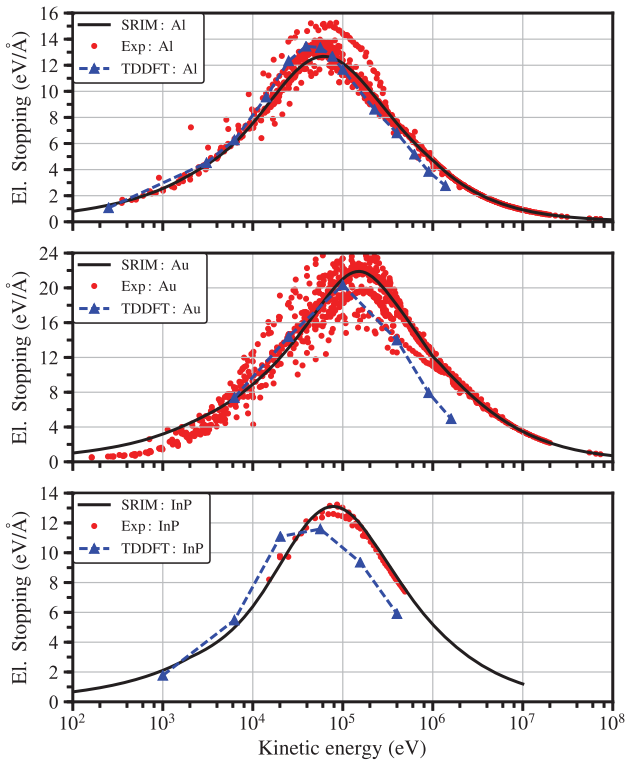

Fig. 6. Electronic stopping for protons impacting Al (top), Au (center), and InP (bottom) targets with different kinetic energies. RT-TDDFT simulations are compared to SRIM data [105] and experiments [108–110].

Matter" [105] (SRIM, see Fig. 6). This work also illustrated the need for modern high-performance supercomputers to perform electron-dynamics simulations for real materials and the requirement of excellent parallelism of simulation codes to benefit from 1 million floating-point processing units or more [106]. We will come back to this in Section 6.

Our recent work focuses on semiconductor target materials: For self-irradiated silicon, we found that the projectile itself leads to local modifications of the electronic structure, causing feedback for electronic stopping of the projectile [107]. The projectile produces defect states in the band structure, and their energetic position depends on the position and local environment of the projectile, possibly contributing to sub-gap electronic stopping.

We investigated stopping of protons in the phosphide-based III-V semiconductors InP (see Fig. 6), GaP, and $In_{0.5}Ga_{0.5}P$ [104]. These are discussed for use in harsh environments including solar panels in outer space as well as radioisotope batteries; however, their lifetime under radiation conditions is a concern. We showed that [001] channeling protons in the ordered CuAu-I phase of $In_{0.5}Ga_{0.5}P$ experience alternating InP/GaP local environments and, thus, local electronic stopping similar to that in InP or GaP. However, at specific velocities, we find enhancement or reduction of local stopping in $In_{0.5}Ga_{0.5}P$ and explain this by contrasting its electron-density distribution with that of pure InP and GaP. This shows how energy levels and spatial electron-density distribution due to the local atomic configuration affect the energy transfer rate during a particle irradiation event.

Furthermore, we find evidence for intricate projectile dynamics in $In_{0.5}Ga_{0.5}P$ [104]: The ordering of In and Ga gives rise to an asymmetric force on the proton on a [001] channel, pushing it from the center of the channel towards the Ga side. Comparing Ehrenfest and Born-Oppenheimer dynamics shows that electronic excitations give rise to larger proton displacement and render proton dynamics velocity-dependent. This non-adiabatic contribution is commonly ignored in the literature but impressively illustrates that electronic excitations need to be taken into account in simulations of radiation damage.

In addition to the discussion of proton stopping for different target materials, Fig. 6 allows us to draw interesting general conclusions regarding the comparison of our data with the commonly used SRIM package [105] or the comparison of SRIM data with experiment. To this end, we lay out specific important limitations of the SRIM model and distinguish three cases based on projectile kinetic energy:

First, as can be seen in Fig. 6, SRIM agrees very well with experimental data points in the high-kinetic energy regime, past the stopping maximum. Thus, in this energy range, agreement with SRIM is a good measure for agreement with experiment. This allowed us previously to attribute deviations of electronic stopping for high-kinetic energy channeling protons from SRIM data to core-electron contributions [99]. These are now well-known and well-studied in the literature for different target materials [99,92,100] and were shown to only matter when impact parameters are not constrained to the channeling case, i.e. when the projectile traverses core regions of target atoms. This can be systematically studied in our simulations and be used to improve the TDDFT description by including core-electron contributions, leading to better agreement with SRIM past the stopping maximum.

Second, for intermediate kinetic energies, near the stopping maximum, Fig. 6 shows that the explicit experimental data points scatter around the SRIM curve. Despite this scattering, the figure shows for several examples that the SRIM curve can be viewed as an average of the experimental data. Hence, comparing to SRIM instead of the explicit experimental data points does not change or bias the interpretation of RT-TDDFT results.

Finally, for low projectile kinetic energies, SRIM is known to show worse agreement with experiment [111]. Reasons for this are well understood in the literature: Due to the overlap of electronic and nuclear stopping in this energy range, it is more difficult to isolate electronic stopping in experiment. Furthermore, in the absence of experimental data, SRIM relies on Bragg's rule of stopping power additivity. This approximation is known [112–114] to overestimate electronic stopping in the low-to-intermediate kinetic-energy range for compounds, i.e. where band-structure effects dominate. Hence, in the low-kinetic energy regime, the agreement of RT-TDDFT results and SRIM is expected to be worse and direct comparison to experiment is preferable, if available.

Recently, we started focusing on non-thermalized energy distributions of electrons associated with particle radiation in materials, and we are studying subsequent non-equilibrium electron-electron and electron-ion dynamics. Early data indicates that electron thermalization itself is not well understood in the context of RT-TDDFT. In order to explore multi-length and time-scale processes triggered by particle radiation, we proposed a first-principles technique that bridges time scales ranging from directly after impact to diffusion of ions [115,116]. By modeling ultrafast electron dynamics and connecting these results to defect migration barriers in semiconductors, we describe a strongly velocity-dependent diffusion mechanism mediated by hot electrons in MgO and estimate the conditions under which it should be observable in experiment [115,116].

6. Integrating time-dependent Kohn-Sham equations in a plane-wave basis

The work in Section 5 is based on RT-TDDFT by integrating TD-KS equations [117,118],

$$i\hbar\frac{\partial}{\partial t}\phi_i\left(\mathbf{r},t\right)=\left\{-\frac{\hbar^2\nabla^2}{2m}+\hat{V}_{\mathrm{ext}}(t)+V_{\mathrm{s}}\left[n(t)\right](\mathbf{r})\right\}\phi_i\left(\mathbf{r},t\right), \tag{6}$$

in real time. Here $\mathbf{r}$ is the spatial coordinate of electrons, t is time, $\phi_i(\mathbf{r},t)$ are KS states, and $V_{\mathrm{s}}[n(t)](\mathbf{r})$ is a functional of the electron density $n(t)$ that describes the Hartree electron-electron interaction and the quantum-mechanical exchange-correlation (XC) potential. For the latter we use the adiabatic local-density approximation (ALDA) [119,120]. The TD potential $\hat{V}_{\mathrm{ext}}(t)$ is given by the ionic system, described by local and non-local parts of the pseudopotential, including

the fast-moving projectile. We first compute the electronic ground state for the equilibrium crystal structure of the target material and then use these KS states and electron density as initial conditions for real-time integration. The Qbox and Qb@ll codes [121,122] are used for numerical simulations.

Integrating TD-KS equations is, however, non-trivial because it requires an efficient, accurate, and highly parallelizable numerical approach. Initially, we implemented a fourth-order Runge-Kutta (FORK) scheme and found satisfactory efficiency and accuracy [123]. While this approach is conditionally stable, we also found that time steps need to be very small, which can partly be attributed to the ultrafast physics of electron dynamics. However, an additional reduction of the time step by a factor of 2 to 10 from the theoretical maximum required for stability is necessary to keep the numerical integration error (e.g. for charge and total energy) small enough for practical applications.

This numerical error of the FORK integrator is controllable by reducing the time step and, more importantly, was largely eliminated when the enforced-time-reversal symmetry (ETRS) integrator was implemented into Qb@ll [106]. Nevertheless, time steps used e.g. for stopping power calculations, are on the order of 1 atto-second (as), imposing severe restrictions on the total simulation time. At the same time, the discussion in Ref. [106] shows excellent parallelization of our code, leading us to conclude that further improvements of parallel scaling prove difficult. Instead, we focus on exploring other integrators to achieve efficiency improvements, greater stability, and smaller numerical error. This is an active field of research [124] with exciting new developments [125,126], also because more flexibility in the integrator is desirable such that propagation remains numerically stable even with advanced XC functionals with increasingly complicated dependence on TD-KS wave functions.

To this end, we recently started exploring a class of integrators that build on Runge-Kutta in order to answer the question of whether it is possible to significantly reduce the time to solution for real-time propagation in a plane-wave context: Strong stability-preserving Runge-Kutta (SSPRK) methods, which are M-stage, N-th order, denoted as SSPRK [127,128]. While these are not specifically designed for time-stepping of TD-KS equations, they have proven successful in achieving small time-stepping errors. We tested the optimal SSPRK(5,4) and SSPRK(10,4) methods, respectively the cheapest and most efficient (in terms of stability, computational expense, and storage requirements) among 4th-order SSPRK methods [127].

To assess the quality of different integrators, we use two figures of merit as well-defined success metrics. First, since numerical integration should ideally conserve charge and change total energy only according to external forces imposed on the system, we evaluate the product of charge and energy error per simulated atto-second ($\Delta Q\,\Delta E$). Second, we also take the integration time step dt and the wall time dT required to perform one such time step into account and evaluate

$$\mathrm{FOM} = \frac{dt}{\Delta Q\,\Delta E\,dT}. \tag{7}$$

Eq. (7) penalizes integrators that require small integration time steps, that lead to large integration errors, and that take a large wall time per simulation time step.

In Fig. 7 we show that for any fixed dt, SSPRK schemes outperform FORK in terms of accuracy and stability. Not only do they enable use of larger time steps and thus decrease time to solution, but they also show a much reduced integration error. This figure also illustrates that the currently implemented ETRS technique performs even better and is the most stable and by far most accurate among the integrators tested. Comparing both subfigures shows that accounting for computational cost does not alter qualitative results for this set of integrators; in particular, the ranking of the integrators remains the same. In order to systematically pursue specialized integrators optimized for TD-KS equations, our recent activities focus on interfacing Qb@ll with the PETSc integrator library [129–132].

Developing integrators and implementing them efficiently into sustainable research software requires interdisciplinary efforts, involving cutting-

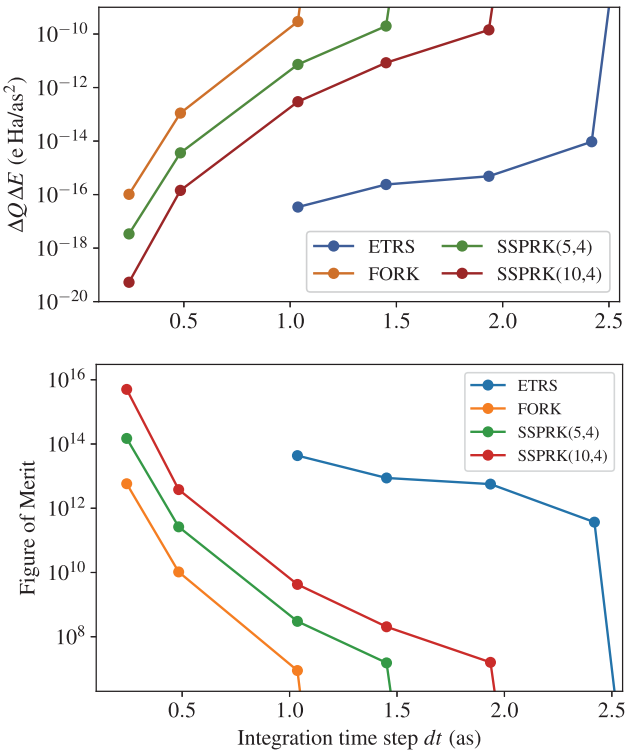

Fig. 7. Comparison of different integrators in RT-TDDFT simulations of a proton impacting a monolayer of graphene. The product of charge and energy error per simulated atto-second (top panel) and the figure of merit (bottom panel, see Eq. (7)) depend on the integration time step.

edge computer science and mathematics knowledge. In addition, fundamental open questions about RT-TDDFT itself remain highly interesting, e.g. regarding limitations of the adiabatic local-density approximation as well as memory effects. This motivates different communities coming together to solve challenging physics, chemistry, and materials science problems, and justifies support across funding agencies as well as international efforts. Achieving this goal has the exciting potential to provide tomorrows' textbook knowledge on fascinating non-equilibrium properties and phenomena that emerge from quantum dynamics in complex systems.

7. Accelerating materials design by incorporating databases

One recurrent theme in this review is that MBPT and TDDFT are accurate and able to capture exciting physics in materials while being computationally expensive. This high cost oftentimes precludes using their predictive capabilities in high-throughput studies, e.g. for materials design, which is however, a desirable goal with tremendous benefit and the potential to solve issues of societal dimension. This motivates us to use our experience with accurate descriptions of electronic excitations to devise techniques capable of studying a significantly larger materials space at manageable computational cost.

One promising route, currently pursued by several groups, is to curate data and incorporate information from materials databases. In particular, computational data based on DFT [135–140] has been used for scintillators [133], optical properties of calcites [141], batteries [142], and solar-cell absorbers [143], to provide a non-exhaustive list of examples. Our particular angle is to exploit DFT-based data to accelerate access to excited-electron properties. Recently, we achieved this to address the important challenge of selecting materials to design multilayer heterojunctions. One of the critical determinants of whether a specific interface between two semiconductors shows beneficial electron or hole transport properties is the offset between valence- and conduction-band edges of the two materials. These band discontinuities are generally not known for an arbitrary interface of two materials due to the difficulty in obtaining this data experimentally or

computationally. However, the overall efficiency of devices strongly depends on energy alignment near the interface.

In our work, we explored whether material properties from ground-state DFT, which are stored for tens of thousands of individual bulk materials, are sufficiently accurate proxies to estimate band alignment between different materials [134]. We computed branch-point energies [144–146] from the freely available bulk electronic band-structure data for all semiconductors in the Materials Project database [135,147]. We then showed that this approach provides band offsets (see Fig. 8) that are comparable in accuracy with available experimental data [148,149] and results from computationally expensive first-principles techniques [146,150–152]. In a similar spirit, branch-point energies were recently used to investigate dopability of materials [153]. Finally, we applied this approach to select optimal material combinations for heterojunctions in specific device applications.

Our alignment is illustrated for all semiconductors on Materials Project in Fig. 8 and shows that many materials are available for a large range of valence- and conduction-band offsets relative to silicon. This data allows us to investigate a staggering number of possible material combinations to form three-component heterojunctions. We demonstrate that this successfully predicts heterojunctions for CdSe and InP LED emitters, solar cells based on bulk $CH_3NH_3PbI_3$ and PbS nanocrystals, and Cu_2O hole-transport layers. In particular, our work shows that although the data on Materials Project results only from ground-state DFT and the branch-point energy is only a rough approximation, this information nevertheless is useful for down-selection from tens of thousands of materials to a few hundred promising candidates. We envision that this approach can be of immense practical importance, not only for novel light-emitting diodes (LEDs), solar cells, and photodetectors, but also for finding two-dimensional electron gases at interfaces as well as electron or hole accumulation near surfaces.

More generally, this shows that computational DFT data in existing online databases is an incredible resource even in the context of excited-electron properties. Building databases, both from experiment and computation, is promising—not just for verification and validation—but also for materials design. Using this information as descriptors and connecting these to materials properties either via analytical models as described above, or via machine-learning techniques, has large potential. To this end, we are exploring collecting experimental data for quantities of interest and then training machine-learning models using descriptors from databases. Taking a step forward, this may allow us to use information gained from materials databases to achieve inverse design [154] and to significantly accelerate materials discovery. Applications that we are currently exploring

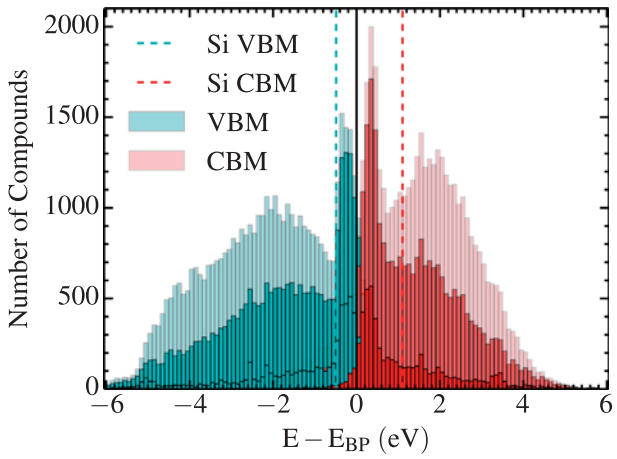

Fig. 8. Comparison of valence-band maximum (VBM) and conduction-band minimum (CBM) positions, aligned using branch-point energies and including band-gap correction (see Refs. [133,134]). 5824 elemental or binary semiconductors (darkest color), 21,202 three-element semiconductors (lighter color), and 45,148 semiconductors (lightest color) from Materials Project are shown. VBM (blue dashed line) and CBM (red dashed line) of silicon are included as a reference.

center around design of nano- and meso-structured meta-materials and heterojunctions and discovery of new superconductors.

8. Conclusions and outlook

Electronic excitations and their ultrafast real-time dynamics are exciting, since experiment and computation push into the spatio-temporal regime of directly probing, controlling, and, thus, understanding them. This justifies vigorous fundamental research, but also motivates the invention and development of novel materials, applications, and devices. This goal relies on a thorough understanding, in part attributed to cutting-edge first-principles techniques. In particular, in this review paper, we illustrated how many-body perturbation theory and time-dependent density-functional theory accomplish accurate predictions for excited electronic states and provide insight into real-time dynamics in modern materials. Through various examples, we discussed how this enabled us to understand the relation between crystal structure and optical absorption, we explained chemical trends, and we connected electronic properties with magnetic ordering. We successfully described energy deposition of fast projectile ions into the electronic system of metallic or semiconducting target materials under radiation conditions.

At the same time, we illustrated that while these techniques are accurate and successful, they necessarily rely on approximations that make them computationally feasible and applicable to complex systems. We discussed exciting ongoing developments to improve their accuracy and make them more applicable: Specifically, dielectric screening needs better theoretical and computational understanding. Integration of time-dependent Kohn-Sham equations was shown to be challenging and imposes restrictions on simulation time. Finally, we discussed incorporating materials databases as an alternate route to mitigate high computational cost of first-principles techniques, e.g. for materials selection, and illustrated this for semiconductor heterojunction design, suggesting a promising down-selection process.

As supercomputers approach the exascale and vast amounts of materials data become openly available, it is an ideal time to harness opportunities that arise. Further pushing accurate and massively parallel first-principles techniques and interfacing with large databases clearly constitute interdisciplinary challenges. However, achieving these will enable computational materials science to deliver fundamental insight from unprecedented predictive simulations, covering multiple length and time scales. We envision that this leads to new materials with applications e.g. in information storage and processing, (quantum) computing, energy, nano-medicine, and at the interface to biology. Transferring those materials into real-world applications will lead to novel and exciting technologies that benefit and transform society.

CRediT authorship contribution statement

Kisung Kang: Conceptualization, Formal analysis, Investigation, Writing - review & editing, Visualization. **Alina Kononov:** Conceptualization, Formal analysis, Investigation, Writing - review & editing, Visualization. **Cheng-Wei Lee:** Conceptualization, Formal analysis, Investigation, Writing - review & editing, Visualization. **Joshua A. Leveillee:** Conceptualization, Formal analysis, Investigation, Writing - review & editing, Visualization. **Ethan P. Shapera:** Conceptualization, Formal analysis, Investigation, Writing - review & editing, Visualization. **Xiao Zhang:** Conceptualization, Formal analysis, Investigation, Writing - review & editing, Visualization. **André Schleife:** Conceptualization, Formal analysis, Investigation, Writing - review & editing, Visualization, Supervision, Project administration, Funding acquisition.

Acknowledgments

We thank Emil Constantinescu, Edoardo di Napoli, Michal Ondrejcek, and Jan Winkelmann for fruitful discussions and Emily Chen

and the NCSA SPIN program for visualization support. This material is based upon work supported by the National Science Foundation under Grant Nos. (DMR-1555153, CBET-1437230, OAC-1740219, and DMR-1720633). Financial support from the Sandia National Laboratories-UIUC collaboration (SNL Grant No. 1736375), the Materials and Manufacturing Graduate Student Fellowship of the National Center for Supercomputing Applications, Los Alamos National Laboratories - Laboratory Directed Research and Development (LANL-LDRD), the Center for Non-Linear Studies, and the Center for Integrated Nano Technology (CNLS and CINT) is acknowledged.

This research is part of the Blue Waters sustained-petascale computing project, which is supported by the National Science Foundation (awards OCI-0725070 and ACI-1238993) and the state of Illinois. Blue Waters is a joint effort of the University of Illinois at Urbana-Champaign and its National Center for Supercomputing Applications. An award of computer time was provided by the Innovative and Novel Computational Impact on Theory and Experiment (INCITE) program. This research used resources of the Argonne Leadership Computing Facility, which is a DOE Office of Science User Facility supported under Contract DE-AC02-06CH11357. This work made use of the Illinois Campus Cluster, a computing resource that is operated by the Illinois Campus Cluster Program (ICCP) in conjunction with the National Center for Supercomputing Applications (NCSA) and which is supported by funds from the University of Illinois at Urbana-Champaign.

References

[1] A. Kogar, M.S. Rak, S. Vig, A.A. Husain, F. Flicker, Y.I. Joe, L. Venema, G.J. MacDougall, T.C. Chiang, E. Fradkin, J. van Wezel, P. Abbamonte, Science 358 (2017) 1314.
[2] S.R. Leone, C.W. McCurdy, J. Burgdorfer, L.S. Cederbaum, Z. Chang, N. Dudovich, J. Feist, C.H. Greene, M. Ivanov, R. Kienberger, U. Keller, M.F. Kling, Z.-H. Loh, T. Pfeifer, A.N. Pfeiffer, R. Santra, K. Schafer, A. Stolow, U. Thumm, M.J.J. Vrakking, Nat. Photon. 8 (2014) 162.
[3] W. Kohn, Rev. Mod. Phys. 71 (1999) 1253.
[4] P. Hohenberg, W. Kohn, Phys. Rev. 136 (1964) B864.
[5] W. Kohn, L.J. Sham, Phys. Rev. 140 (1965) A1133.
[6] D.M. Ceperley, B.J. Alder, Phys. Rev. Lett. 45 (1980) 566.
[7] J.P. Perdew, K. Burke, M. Ernzerhof, Phys. Rev. Lett. 77 (1996) 3865.
[8] E. Runge, E.K.U. Gross, Phys. Rev. Lett. 52 (1984) 997.
[9] G. Onida, L. Reining, A. Rubio, Rev. Mod. Phys. 74 (2002) 601.
[10] L. Hedin, Phys. Rev. 139 (1965) A796.
[11] S. Louie, S.G. Louie, M.L. Cohen (Eds.), Conceptual Foundations of Materials Contemporary Concepts of Condensed Matter Science, vol. 2, Elsevier, 2006, pp. 9–53 (Chapter 2).
[12] A. Seidl, A. Görling, P. Vogl, J.A. Majewski, M. Levy, Phys. Rev. B 53 (1996) 3764.
[13] J. Heyd, G.E. Scuseria, M. Ernzerhof, J. Chem. Phys. 124 (2006) 219906.
[14] P.H. Hahn, W.G. Schmidt, F. Bechstedt, Phys. Rev. Lett. 88 (2001) 016402.
[15] W.G. Schmidt, S. Glutsch, P.H. Hahn, F. Bechstedt, Phys. Rev. B 67 (2003) 085307.
[16] F. Fuchs, C. Rödl, A. Schleife, F. Bechstedt, Phys. Rev. B 78 (2008) 085103.
[17] M. Gajdoš, K. Hummer, G. Kresse, J. Furthmüller, F. Bechstedt, Phys. Rev. B 73 (2006) 045112.
[18] G. Kresse, D. Joubert, Phys. Rev. B 59 (1999) 1758.
[19] G. Kresse, J. Furthmüller, Phys. Rev. B 54 (1996) 11169.
[20] M. Shishkin, G. Kresse, Phys. Rev. B 74 (2006) 035101.
[21] C. Rödl, F. Fuchs, J. Furthmüller, F. Bechstedt, Phys. Rev. B 77 (2008) 184408.
[22] F. Bechstedt, R.D. Sole, G. Cappellini, L. Reining, Solid State Commun. 84 (1992) 765.
[23] A. Schleife, F. Fuchs, J. Furthmüller, F. Bechstedt, Phys. Rev. B 73 (2006) 245212.
[24] A. Schleife, C. Rödl, F. Fuchs, J. Furthmüller, F. Bechstedt, P.H. Jefferson, T.D. Veal, C.F. McConville, L.F.J. Piper, A. DeMasi, K.E. Smith, H. Lösch, R. Goldhahn, C. Cobet, J. Zúñiga-Pérez, V. Muñoz-Sanjosé, J. Korean Phys. Soc. 53 (2008) 2811.
[25] A. Schleife, C. Rödl, F. Fuchs, J. Furthmüller, F. Bechstedt, Phys. Rev. B 80 (2009) 035112.
[26] A. Schleife, J.B. Varley, F. Fuchs, C. Rödl, F. Bechstedt, P. Rinke, A. Janotti, C.G. Van de Walle, Phys. Rev. B 83 (2011) 035116.
[27] A. Schleife, F. Bechstedt, J. Mater. Res. 27 (2012) 2180.
[28] S. Küfner, A. Schleife, B. Höffling, F. Bechstedt, Phys. Rev. B 86 (2012) 075320.
[29] J. Furthmüller, F. Hachenberg, A. Schleife, D. Rogers, F.H. Teherani, F. Bechstedt, Appl. Phys. Lett. 100 (2012) 022107.
[30] L.C. de Carvalho, A. Schleife, F. Bechstedt, Phys. Rev. B 84 (2011) 195105.
[31] A. Belabbes, L.C. de Carvalho, A. Schleife, F. Bechstedt, Phys. Rev. B 84 (2011) 125108.
[32] A. Schleife, F. Fuchs, C. Rödl, J. Furthmüller, F. Bechstedt, Phys. Status Solidi B 246 (2009) 2150.
[33] L.C. de Carvalho, A. Schleife, F. Fuchs, F. Bechstedt, Appl. Phys. Lett. 97 (2010) 232101.
[34] A. Schleife, P. Rinke, F. Bechstedt, C.G. Van de Walle, J. Phys. Chem. C 117 (2013) 4189.
[35] A. Schleife, M. Eisenacher, C. Rödl, F. Fuchs, J. Furthmüller, F. Bechstedt, Phys. Rev. B 81 (2010) 245210.
[36] A. Schleife, C. Rödl, J. Furthmüller, F. Bechstedt, New J. Phys. 13 (2011) 085012.
[37] S.K.V. Farahani, C.F. McConville, T.D. Veal, A. Schleife, Proc. SPIE 8626 (2013) 862604.
[38] L.C. de Carvalho, A. Schleife, J. Furthmüller, F. Bechstedt, Phys. Rev. B 85 (2012) 115121.
[39] L.C. de Carvalho, A. Schleife, J. Furthmüller, F. Bechstedt, Phys. Rev. B 87 (2013) 195211.
[40] P. Rinke, A. Schleife, E. Kioupakis, A. Janotti, C. Rödl, F. Bechstedt, M. Scheffler, C.G. Van de Walle, Phys. Rev. Lett. 108 (2012) 126404.
[41] J.B. Varley, A. Schleife, Semicond. Sci. Technol. 30 (2015) 024010.
[42] J.-X. Shen, A. Schleife, A. Janotti, C.G. Van de Walle, Phys. Rev. B 94 (2016) 205203.
[43] R.D. McAuliffe, C.A. Miller, X. Zhang, B.S. Hulbert, A. Huq, C. dela Cruz, A. Schleife, D.P. Shoemaker, Inorg. Chem. 56 (2017) 2914.
[44] A. Schleife, X. Zhang, Q. Li, P. Erhart, D. Åberg, J. Mater. Res. 32 (2017) 56.
[45] P. Erhart, A. Schleife, B. Sadigh, D. Åberg, Phys. Rev. B 89 (2014) 075132.
[46] A. McAllister, D. Åberg, A. Schleife, E. Kioupakis, Appl. Phys. Lett. 106 (2015) 141901.
[47] X. Zhang, A. Schleife, Phys. Rev. B 97 (2018) 125201.
[48] F. Claeyssens, C.L. Freeman, N.L. Allan, Y. Sun, M.N.R. Ashfold, J.H. Harding, J. Mater. Chem. 15 (2005) 139.
[49] C.L. Freeman, F. Claeyssens, N.L. Allan, J.H. Harding, Phys. Rev. Lett. 96 (2006) 066102.
[50] B. Liu, J.A. Boscoboinik, Y. Cui, S. Shaikhutdinov, H. Freund, J. Phys. Chem. C 119 (2015) 7842.
[51] C.L. Pueyo, S. Siroky, S. Landsmann, M.W.E. van den Berg, M.R. Wagner, J.S. Reparaz, A. Hoffmann, S. Polarz, Chem. Mater. 22 (2010) 4263.
[52] B. Rakshit, P. Mahadevan, Phys. Rev. Lett. 107 (2011) 085508.
[53] D. Zagorac, J.C. Schön, J. Zagorac, M. Jansen, Phys. Rev. B 89 (2014) 075201.
[54] B. Rakshit, P. Mahadevan, Appl. Phys. Lett. 102 (2013) 143116.
[55] J.E. Jaffe, J.A. Snyder, Z. Lin, A.C. Hess, Phys. Rev. B 62 (2000) 1660.
[56] O.S. Heavens, Rep. Prog. Phys. 23 (1960) 1.
[57] S.J. Orfanidis, Electromagnetic Waves and Antennas, Rutgers University New Brunswick, NJ, 2002.
[58] S.J. Lim, A. Schleife, A.M. Smith, Nat. Commun. 8 (2017) 14849.
[59] J. Leveillee, C. Katan, L. Zhou, A. Mohite, J. Even, S. Tretiak, A. Schleife, A.J. Neukirch, Phys. Rev. Mater. (2018).
[60] L. Pedesseau, D. Sapori, B. Traore, R. Robles, H.-H. Fang, M.A. Loi, H. Tsai, W. Nie, J.-C. Blancon, A. Neukirch, S. Tretiak, A.D. Mohite, C. Katan, J. Even, M. Kepenekian, ACS Nano 10 (2016) 9776.
[61] H. Tsai, W. Nie, J.-C. Blancon, C.C. Stoumpos, R. Asadpour, B. Harutyunyan, A.J. Neukirch, R. Verduzco, J.J. Crochet, S. Tretiak, L. Pedesseau, J. Even, M.A. Alam, G. Gupta, J. Lou, P.M. Ajayan, M.J. Bedzyk, M.G. Kanatzidis, A.D. Mohite, Nature 536 (2016) 312.
[62] H. Tsai, W. Nie, J.-C. Blancon, C.C. Stoumpos, C.M.M. Soe, J. Yoo, J. Crochet, S. Tretiak, J. Even, A. Sadhanala, G. Azzellino, R. Brenes, P.M. Ajayan, V. Bulović, S.D. Stranks, R.H. Friend, M.G. Kanatzidis, A.D. Mohite, Adv. Mater. 30 (2018) 1704217.
[63] L. Šmejkal, J. Železný, J. Sinova, T. Jungwirth, Phys. Rev. Lett. 118 (2017) 106402.
[64] X.-L. Li, X. Duan, Y.G. Semenov, K.W. Kim, J. Appl. Phys. 121 (2017) 023907.
[65] Y. Kim, K. Kang, A. Schleife, M.J. Gilbert, Phys. Rev. B 97 (2018) 134415.
[66] M. Born, J.R. Oppenheimer, Ann. Phys. 389 (1927) 457.
[67] R. Del Sole, R. Girlanda, Phys. Rev. B 48 (1993) 11789.
[68] A. Schleife, C. Rödl, F. Fuchs, J. Furthmüller, F. Bechstedt, Appl. Phys. Lett. 91 (2007) 241915.
[69] C. Wagner, J. Schuster, A. Schleife, 2018, arXiv: 1801.04712.
[70] A. Schleife, F. Bechstedt, Proc. SPIE 8263 (2012) 826309.
[71] C. Rödl, A. Schleife, Phys. Status Solidi A 211 (2014) 74.
[72] A. Kronenberger, A. Polity, D.M. Hofmann, B.K. Meyer, A. Schleife, F. Bechstedt, Phys. Rev. B 86 (2012) 115334.
[73] A. Schleife, Exciting Imperfection: Real-structure Effects in Magnesium-, Cadmium-, and Zinc-oxide (Ph.D. thesis), Friedrich-Schiller-Universität, Jena, 2010.
[74] A. Schleife, Electronic and Optical Properties of MgO, ZnO, and CdO, Südwestdeutscher Verlag für Hochschulschriften, 2011.
[75] A. Schleife, C. Rödl, F. Fuchs, K. Hannewald, F. Bechstedt, Phys. Rev. Lett. 107 (2011) 236405.
[76] F. Giustino, Rev. Mod. Phys. 89 (2017) 015003.
[77] S. Botti, M.A.L. Marques, Phys. Rev. Lett. 110 (2013) 226404.
[78] W.R.L. Lambrecht, C. Bhandari, M. van Schilfgaarde, Phys. Rev. Mater. 1 (2017) 043802.
[79] J.P. Nery, P.B. Allen, Phys. Rev. B 94 (2016) 115135.
[80] F. Bechstedt, K. Seino, P.H. Hahn, W.G. Schmidt, Phys. Rev. B 72 (2005) 245114.
[81] F. Bechstedt, Beyond static screening, Many-Body Approach to Electronic Excitations: Concepts and Applications, Springer Berlin Heidelberg, Berlin, Heidelberg, 2015, pp. 539–572.
[82] R.H. Lyddane, R.G. Sachs, E. Teller, Phys. Rev. 59 (1941) 673.
[83] A. Schleife, M.D. Neumann, N. Esser, Z. Galazka, A. Gottwald, J. Nixdorf, R. Goldhahn, M. Feneberg, New J. Phys. 20 (2018) 053016.
[84] Q. Wang, Y. Shao, H. Xie, L. Lyu, X. Liu, Y. Gao, J. Huang, Appl. Phys. Lett. 105

(2014) 163508.
[85] L.A. Frolova, N.N. Dremova, P.A. Troshin, Chem. Commun. 51 (2015) 14917.
[86] O.E. Semonin, G.A. Elbaz, D.B. Straus, T.D. Hull, D.W. Paley, A.M. van der Zande, J.C. Hone, I. Kymissis, C.R. Kagan, X. Roy, J.S. Owen, J. Phys. Chem. Lett. 7 (2016) 3510.
[87] J. Winkelmann, P. Springer, E.D. Napoli, 2018, arXiv: 1805.10121.
[88] M. Shao, F. da Jornada, L. Lin, C. Yang, J. Deslippe, S. Louie, SIAM J. Matrix Anal. Appl. 39 (2018) 683.
[89] M.A. Marques, N.T. Maitra, F.M. Nogueira, E. Gross, A. Rubio (Eds.), Fundamentals of Time-Dependent Density Functional Theory, Springer, 2012.
[90] C.A. Ullrich (Ed.), Time-Dependent Density-Functional Theory: Concepts and Applications, Oxford University Press, 2012.
[91] A.A. Correa, Comput. Mater. Sci. 150 (2018) 291.
[92] D.C. Yost, Y. Yao, Y. Kanai, Phys. Rev. B 96 (2017) 115134.
[93] R. Ullah, E. Artacho, A.A. Correa, Phys. Rev. Lett. 121 (2018) 116401.
[94] A. Ojanperä, A.V. Krasheninnikov, M. Puska, Phys. Rev. B 89 (2014) 035120.
[95] M. Quijada, A.G. Borisov, I. Nagy, R.D. Muiño, P.M. Echenique, Phys. Rev. A 75 (2007) 042902.
[96] Z. Wang, S.-S. Li, L.-W. Wang, Phys. Rev. Lett. 114 (2015) 063004.
[97] A.V. Krasheninnikov, Y. Miyamoto, D. Tománek, Phys. Rev. Lett. 99 (2007) 016104.
[98] A.A. Correa, J. Kohanoff, E. Artacho, D. Sánchez-Portal, A. Caro, Phys. Rev. Lett. 108 (2012) 213201.
[99] A. Schleife, Y. Kanai, A.A. Correa, Phys. Rev. B 91 (2015) 014306.
[100] E.E. Quashie, B.C. Saha, A.A. Correa, Phys. Rev. B 94 (2016) 155403.
[101] A. Schleife, E.W. Draeger, V. Anisimov, A.A. Correa, Y. Kanai, Comput. Sci. Eng. 16 (2014) 54.
[102] J.M. Pruneda, D. Sánchez-Portal, A. Arnau, J.I. Juaristi, E. Artacho, Phys. Rev. Lett. 99 (2007) 235501.
[103] C.-K. Li, F. Wang, B. Liao, X.-P. OuYang, F.-S. Zhang, Phys. Rev. B 96 (2017) 094301.
[104] C.-W. Lee, A. Schleife, Eur. Phys. J. B 91 (2018) 222.
[105] J.F. Ziegler, M.D. Ziegler, J.P. Biersack, Nucl. Instrum. Meth. B 268 (2010) 1818.
[106] E.W. Draeger, X. Andrade, J.A. Gunnels, A. Bhatele, A. Schleife, A.A. Correa, J. Par. Distr. Comp. 106 (2017) 205.
[107] A. Lim, W.M.C. Foulkes, A.P. Horsfield, D.R. Mason, A. Schleife, E.W. Draeger, A.A. Correa, Phys. Rev. Lett. 116 (2016) 043201.
[108] V.A. Khodyrev, V.N. Mizgulin, E.I. Sirotinin, A.F. Tulinov, Radiat. Eff. 83 (1984) 21.
[109] International Atomic Energy Agency Nuclear Data Services, Stopping Power of Matter for Ions: Hydrogen Ions, Data retrieved from https://www-nds.iaea.org/stopping/stopping_hydr.html.
[110] S.R. Lee, R. Hart, Nucl. Instrum. Meth. B 28 (1987) 470.
[111] H. Paul, A. Schinner, Nucl. Instrum. Meth. B 227 (2005) 461.
[112] J.S.-Y. Feng, W.K. Chu, M.A. Nicolet, Phys. Rev. B 10 (1974) 3781.
[113] R.A. Langley, R.S. Blewer, Nucl. Instrum. Meth. 132 (1976) 109.
[114] I. Abril, R. Garcia-Molina, N.R. Arista, C.F. Sanz-Navarro, Nucl. Instrum. Meth. B 190 (2002) 89.
[115] C.-W. Lee, A. Schleife, Mater. Today 21 (2018) 925.
[116] C.-W. Lee, A. Schleife, 2018, arXiv: 1806.00443.
[117] V. Peuckert, J. Phys. C 11 (1978) 4945.
[118] A. Zangwill, P. Soven, Phys. Rev. A 21 (1980) 1561.
[119] A. Zangwill, P. Soven, Phys. Rev. B 24 (1981) 4121.
[120] A. Zangwill, P. Soven, Phys. Rev. Lett. 45 (1980) 204.
[121] F. Gygi, IBM J. Res. Dev. 52 (2008) 137.
[122] E.W. Draeger, F. Gygi, Qbox code, qb@ll version, Lawrence Livermore National Laboratory, 2017.
[123] A. Schleife, E.W. Draeger, Y. Kanai, A.A. Correa, J. Chem. Phys. 137 (2012) 22A546.
[124] A. Gómez Pueyo, M.A.L. Marques, A. Rubio, A. Castro, J. Chem. Theor. Comput. 14 (2018) 3040.
[125] W. Jia, D. An, L.-W. Wang, L. Lin, 2018, arXiv: 1805.10575.
[126] D. An, L. Lin, 2018, arXiv: 1804.02095.
[127] S. Gottlieb, D.I. Ketcheson, C.-W. Shu, J. Sci. Comput. 38 (2009) 251.
[128] S. Gottlieb, Strong Stability Preserving Runge-Kutta and Multistep Time Discretizations, World Scientific, 2010.
[129] S. Abhyankar, J. Brown, E.M. Constantinescu, D. Ghosh, B.F. Smith, H. Zhang, 2018, arXiv: 1806.01437.
[130] S. Balay, W.D. Gropp, L.C. McInnes, B.F. Smith, E. Arge, A.M. Bruaset, H.P. Langtangen (Eds.), Modern Software Tools in Scientific Computing, Birkhäuser Press, 1997, pp. 163–202.
[131] S. Balay, S. Abhyankar, M.F. Adams, J. Brown, P. Brune, K. Buschelman, L. Dalcin, A. Dener, V. Eijkhout, W.D. Gropp, D. Kaushik, M.G. Knepley, D.A. May, L.C. McInnes, R.T. Mills, T. Munson, K. Rupp, P. Sanan, B.F. Smith, S. Zampini, H. Zhang, H. Zhang, PETSc Web page, 2018a. http://www.mcs.anl.gov/petsc.
[132] S. Balay, S. Abhyankar, M.F. Adams, J. Brown, P. Brune, K. Buschelman, L. Dalcin, A. Dener, V. Eijkhout, W.D. Gropp, D. Kaushik, M.G. Knepley, D.A. May, L.C. McInnes, R.T. Mills, T. Munson, K. Rupp, P. Sanan, B.F. Smith, S. Zampini, H. Zhang, H. Zhang, PETSc Users Manual, Tech. Rep. ANL-95/11 - Revision 3.10 (Argonne National Laboratory, 2018).
[133] W. Setyawan, R.M. Gaume, S. Lam, R.S. Feigelson, S. Curtarolo, ACS Comb. Sci. 13 (2011) 382.
[134] E.P. Shapera, A. Schleife, Adv. Theor. Simul. 1 (2018) 1800075.
[135] A. Jain, S.P. Ong, G. Hautier, W. Chen, W.D. Richards, S. Dacek, S. Cholia, D. Gunter, D. Skinner, G. Ceder, K.A. Persson, APL Mater. 1 (2013) 011002.
[136] R.H. Taylor, F. Rose, C. Toher, O. Levy, K. Yang, M.B. Nardelli, S. Curtarolo, Comput. Mater. Sci. 93 (2014) 178.
[137] J.E. Saal, S. Kirklin, M. Aykol, B. Meredig, C. Wolverton, JOM 65 (2013) 1501.
[138] C. Ortiz, O. Eriksson, M. Klintenberg, Comput. Mater. Sci. 44 (2009) 1042.
[139] M. Scheffler, C. Draxl, Computer center of the max-planck society, garching, the nomad repository, 2014, https://nomad-repository.eu/.
[140] G. Pizzi, A. Cepellotti, R. Sabatini, N. Marzari, B. Kozinsky, Comput. Mater. Sci. 111 (2016) 218.
[141] K.M. Poduska, L. Regev, E. Boaretto, L. Addadi, S. Weiner, L. Kronik, S. Curtarolo, Adv. Mater. 23 (2011) 550.
[142] M.N. Obrovac, V.L. Chevrier, Chem. Rev. 114 (2014) 11444.
[143] L. Yu, A. Zunger, Phys. Rev. Lett. 108 (2012) 068701.
[144] J. Tersoff, Phys. Rev. B 30 (1984) 4874.
[145] A. Schleife, F. Fuchs, C. Rödl, J. Furthmüller, F. Bechstedt, Appl. Phys. Lett. 94 (2009) 012104.
[146] Y. Hinuma, A. Grüneis, G. Kresse, F. Oba, Phys. Rev. B 90 (2014) 155405.
[147] S.P. Ong, W.D. Richards, A. Jain, G. Hautier, M. Kocher, S. Cholia, D. Gunter, V.L. Chevrier, K.A. Persson, G. Ceder, Comput. Mater. Sci. 68 (2013) 314.
[148] W. Mönch, Electronic Properties of Semiconductor Interfaces, Springer, Berlin, 2004.
[149] D. Mourad, J.-P. Richters, L. Gérard, R. André, J. Bleuse, H. Mariette, Phys. Rev. B 86 (2012) 195308.
[150] B. Höffling, A. Schleife, F. Fuchs, C. Rödl, F. Bechstedt, Appl. Phys. Lett. 97 (2010) 032116.
[151] B. Höffling, A. Schleife, C. Rödl, F. Bechstedt, Phys. Rev. B 85 (2012) 035305.
[152] C.G. Van de Walle, J. Neugebauer, Nature 423 (2003) 626.
[153] R. Woods-Robinson, D. Broberg, A. Faghaninia, A. Jain, S.S. Dwaraknath, K.A. Persson, Chem. Mater. 30 (2018) 8375.
[154] A. Zunger, Nat. Rev. Chem. 2 (2018) 0121.